Complex Hydrides for Electrochemical Energy Storage

*Atsushi Unemoto, Motoaki Matsuo, and Shin-ichi Orimo**

Complex hydrides have energy storage-related functions such as i) solid-state hydrogen storage, ii) electrochemical Li storage, and iii) fast Li- and Na-ionic conductions. Here, recent progress on the development of fast Li-ionic conductors based on the complex hydrides is reported. The validity of using them as electrolytes in all-solid-state lithium rechargeable batteries is also examined. Not only coated oxides but also bare sulfides are found to be applicable as positive electrode active materials. Results related to fast Na-ionic conductivity in the complex hydrides are presented. In the last section, the future prospects for battery assemblies with high-energy densities, and Mg ion batteries with the liquid and the solid-state electrolytes are discussed.

1. Introduction

Complex hydrides consisting of a metal cation and a complex anion are represented by the formula, $M(M'Hn)$. Here examples of the metal cation, M, are Li^+, Na^+, Mg^{2+}, and so forth, and those of the complex anion, $M'Hn$, are $[BH_4]^-$, $[NH_2]^-$, $[AlH_4]^-$, $[AlH_6]^{3-}$, and so on.[1]

$LiBH_4$ is a typical complex hydride formed by ionic bonding between Li^+ and complex anion, $[BH_4]^-$. Despite the conventional applications of $LiBH_4$ in chemical processes as a reducing agent, energy storage-related functions such as i) solid-state hydrogen storage, ii) electrochemical Li storage, and iii) fast Li- and Na-ionic conductions are focused on the class of the materials.

i) Solid-state hydrogen storage: This is the most classical energy-conversion related function. $LiBH_4$ possesses high gravimetric and volumetric hydrogen densities compared to the other hydrogen storage materials.[1–4] $LiBH_4$ experiences the phase transition from low-temperature (LT) phase (orthorhombic structure with a space group of *Pnma*, shown in **Figure 1**a) to high-temperature (HT) one (hexagonal structure with a space group of $P6_3mc$, shown in Figure 1b) at approximately 390 K. $LiBH_4$ releases approximately 13.8 mass % hydrogen via the following decomposition reaction,[1,2,4]

$$LiBH_4 \rightleftharpoons LiH + B + 3/2H_2 \quad (1)$$

Despite its high hydrogen density, slow dehydriding and rehydriding kinetics interfere with its practical application. To enhance the slow dehydriding and rehydriding kinetics, researchers have proposed the introduction of additives.[5] Confinements in structured carbons[6–9] as well as the introduction of the intermediate reactions with the reactive media[10–15] are also reported to be effective measures.

ii) Electrochemical Li storage: Oumellal et al. first reported the reversible electrochemical conversion reaction of the redox couple, MgH_2/Li.[17] It exhibits a reversible capacity of 1480 mAh g^{-1} at an average voltage of 0.5 V versus Li/Li^+.[18–20] Developments have extended not only to other metal hydrides, that is, TiH_2[19,21] and AlH_3,[20] but also to transition-metal-based complex hydrides such as Mg_2FeH_6, Mg_2CoH_5, and Mg_2NiH_4.[22,23] These materials exhibit higher theoretical gravimetric and volumetric capacities than the conventional graphite negative electrode (**Figure 2**). The electrochemical conversion reaction of the transition-metal complex hydrides, as exemplified by Mg_2FeH_6, proceeds as in the literature.[22,23]

$$Mg_2FeH_6 + 6Li^+ + 6e- \rightleftharpoons 6LiH + 2Mg + Fe \quad (2)$$

Optimization of the composite electrode structure need to be addressed to mitigate the overpotential accompanied by the slow conversion kinetics.[22]

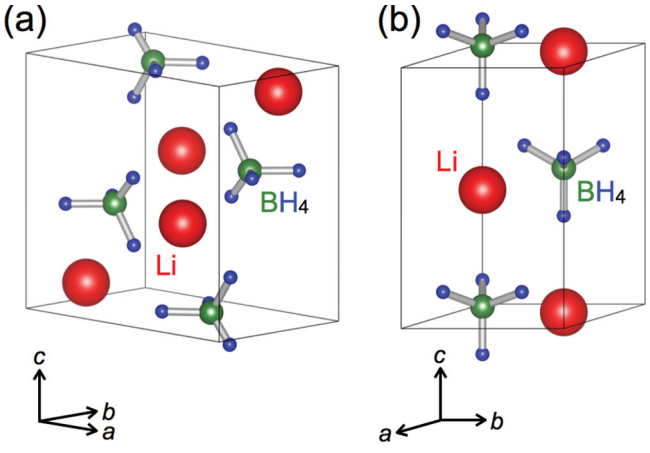

Figure 1. Crystal structures of a) LT phase and b) HT phase of $LiBH_4$.[16]

Prof. A. Unemoto, Prof. S. Orimo
WPI-Advanced Institute for Materials Research
Tohoku University
Sendai, Japan
E-mail: orimo@imr.tohoku.ac.jp
Prof. M. Matsuo, Prof. S. Orimo
Institute for Materials Research
Tohoku University
Sendai, Japan

DOI: 10.1002/adfm.201303147

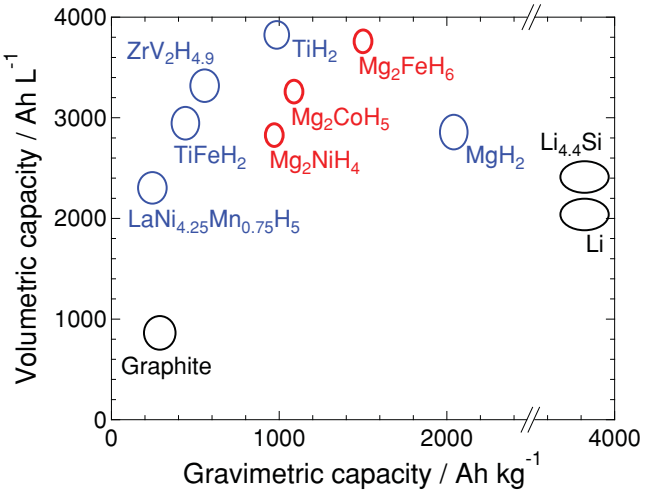

Figure 2. Gravimetric and volumetric capacities of metal hydrides and metal complex hydrides compared with those of graphite and other negative electrode materials. Reproduced with permission.[22] Copyright 2011, International Association of Hydrogen Energy.

iii) Fast Li- and Na-ionic conductions: One of the important challenges in the field of battery research is the development of fast ionic conductors because this class of materials enables the assembly from micro-[24] to bulk-type[25–27] all-solid-state rechargeable cells, which allows the broader applications. With this background, various solid-state electrolytes have been developed so far, however, the materials showing sufficient ionic conductivity as well as good stability in the voltage ranges for battery operation are limited to a few cases.[28] Therefore, novel solid-state electrolytes are urgently required for the development of future generation batteries. Since the discovery of fast Li-ionic conduction in the HT phase of $LiBH_4$,[29] we have developed numerous solid-state electrolytes based on the complex hydrides that exhibit fast Li- and Na-ionic conductions.[30]

Herein, we briefly report recent progress in the development of the complex hydrides that exhibit fast Li-ionic conduction. All-solid-state Li rechargeable batteries were subsequently assembled using coated-$LiCoO_2$ and TiS_2 positive electrodes, and $LiBH_4$-based electrolytes. The validity of the use of the complex hydrides as electrolytes in a rechargeable battery was examined on the basis of charge–discharge measurements. In the following section, our recent development of fast Na-ionic conductors based on the complex hydrides is summarized. We discuss the future prospects for the development of high energy density rechargeable batteries, and Mg-ion batteries that use nonaqueous and solid-state electrolytes based on the complex hydrides.

2. Rechargeable Li-Ion Battery Development Using Complex Hydride-Based Fast Li-Ionic Conductors

Complex hydrides are now considered possible candidates as solid-state electrolytes in all-solid-state rechargeable batteries. In addition to fast Li-ionic conduction, the advantages of the use of complex hydrides as rechargeable battery electrolytes are as follows,

Atsushi Unemoto received his PhD. in environmental studies from Tohoku University in 2009. He was a JSPS research fellow (2008–2009), an assistant professor at the Graduate School of Engineering, Tohoku University (2009–2010), and at the Institute of Multidisciplinary Research for Advanced Materials, Tohoku University (2010–2013). He is currently a lecturer at the Advanced Institute for Materials Research (WPI-AIMR), Tohoku University. His research interests are the solid-state electrochemistry and solid-state ionics for electrochemical energy-conversion devices.

Motoaki Matsuo received his Ph.D. in materials science in 2008 from Tohoku University. He worked as a postdoctoral fellow (2008–2010) and as an assistant professor (2010–2012), and is currently a lecturer in the Orimo group at the Institute for Materials Research, Tohoku University. His research interests are the fundamental, physical, and chemical properties of light-weight hydrides, particularly solid-state ionics, and hydrogen storage.

Shin-ichi Orimo received his Ph.D. in materials science/physics from Hiroshima University in 1995. He was a JSPS research fellow (1993–1995), a research associate in Hiroshima University (1995–2002), and a guest researcher at the Max-Planck Institute for Metal Research for which he was funded by a Alexander von Humboldt Fellowship and a MEXT Fellowship (1998–1999). He is currently a professor at the Advanced Institute for Materials Research (as a Principal Investigator) and the Institute of Materials Research (as a Head of Section), Tohoku University. His research interests are fundamentals and energy-related applications of hydrides, particularly hydrogen storage and solid-state ionics.

1) Light weight: Densities of the complex hydrides are lower than those of oxides and sulfides (Table S1– S4, Supporting Information). It is advantageous for the development of light weight devices, and allows the increased concentration of the active materials in composite electrodes.
2) High compatibility with Li and Na electrodes: The complex hydrides form a reversible and stable interface with Li[29,31] and Na electrodes[32,33] during metal deposition and stripping, and battery operation. In addition, the ac impedance spectra of Li and Na symmetric cells consist of only one semicircle attributed to the electrolyte resistance. Giving a uniaxial pressure by a spring in an electrochemical cell is sufficient to form the reversible interface between the complex hydrides and metallic electrodes.[29,31–33]
3) High chemical stability: The complex hydrides have wide potential windows. They are stable in not only reducing environment but also oxidizing one such as at potentials greater than 5 V vs Li/Li^+[30] and 6 V vs Na/Na^+.[32] As will be described in the following subsections, the all-solid-state cells assembled using the $LiBH_4$-based solid-state electrolytes could be operated at least for 10–30 charge - discharge cycles with high Coulombic efficiency. This implies that the complex hydride-based solid-state electrolyte is stable during the battery operation.
4) High thermal stability: Due to the strong covalency between the metals and non-metals with hydrogen in a complex anion, decomposition hardly proceeds even at higher temperatures.[1–4]
5) Easy to form the electrode/electrolyte interface: The formation of a preferable interface consisting of the active material and electrolyte particles by simple uniaxial pressing is straightforward owing to the highly deformable nature of the complex hydrides. Details of this feature are discussed together with the microstructure observations of the cross-section of the composite positive electrode in the next section.

First, we present our recent development related to fast Li-ionic conductors. Then, in the following subsequent section, we report our recent works on the all-solid-state Li rechargeable battery assembly.

2.1. Fast Li-Ionic Conductors

$LiBH_4$ undergoes a phase transition at approximately 390 K. The HT phase exhibits fast Li-ionic conductivity of greater than 2×10^{-3} S cm^{-1},[29] as shown in **Figure 3** (the numerical data are summarized in Table S5, Supporting Information). Large band gaps with approximately 6 eV both in the LT- and HT-phase of $LiBH_4$[49,50] suggests the negligible contribution of the electronic conductivity in that material.

The primary approach for the development of solid-state electrolytes is to stabilize the HT phase of $LiBH_4$ in the lower temperature region even at room temperature. This stabilization could be achieved through the partial replacement of the complex anion, $[BH_4]^-$ (0.205 nm), by iodide-ions, I^- (0.211 nm). Accompanied by the increasing of the I^- doping level, the phase transition temperature monotonically decreased.[51,52] As a result, the solid-solution, $Li(BH_4)_{1-x}I_x$, maintains the

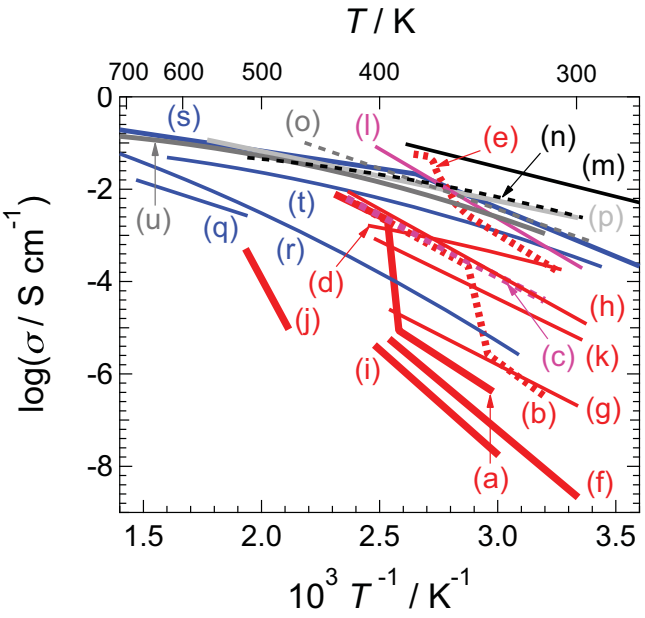

Figure 3. Electrical conductivities of various Li-ion conducting solids as functions of the inverse temperature: a) $LiBH_4$,[29] b) $Li_4(BH_4)3Cl$,[34,35] c) $Li_4(BH_4)_3I$,[34] d) $Li_4(BH_4)(NH_2)_3$,[36] e) $Li_2(BH_4)(NH_2)$,[36] f) $LiAlH_4$,[31] g) Li_3AlH_6,[31] h) $Li_3(NH_2)_2I$,[37] i) $LiNH_2$,[38] j) $Li_2Mg(NH_2)_2$,[38] k) $Li_2Ca(NH)_2$,[38] l) Li_2NH,[38,120] m) $Li_{10}GeP_2S_{12}$,[39] n) $Li_7P_3S_{11}$ (glass-ceramics),[40] o) Li_2S-SiS_2-Li_3PO_4 (glass),[41,42] p) $Li_{0.325}Ge_{0.25}P_{0.75}S_4$ (thio-LISICON),[43] q) Li-beta-alumina,[44] r) $Li_{14}Zn(GeO_4)_4$ (LISICON),[45] s) $Li_{0.34}La_{0.51}TiO_{2.94}$,[46,130] t) $Li_7La_3Zr_2O_{12}$,[47,129] and u) $Li_{1.3}Al_{0.3}Ti_{1.7}(PO_4)_3$ (LATP).[48]

hexagonal phase of $LiBH_4$ (fast Li-ion conduction phase) even at room temperature when x exceeds 0.25. And then, the solid-solution, $Li_4(BH_4)_3I$, exhibits fast Li-ionic conductivity of 2×10^{-5} S cm^{-1} at 300 K.[34,51–53] This phenomenon might be due to increased neighboring distance of $[BH_4]^-$[54] and induced lattice anharmonicity by the partial substitution of I^- instead of $[BH_4]^-$.[55,56]

We extended our research and development to the pseudo-ternary system consisting of $LiBH_4$-$LiNH_2$-LiI.[36,37] As a result, we successfully developed the complex hydrides that exhibit fast Li-ionic conductivity including $Li_2(BH_4)(NH_2)$, $Li_4(BH_4)(NH_2)_3$[36] and $Li_3(NH_2)_2I$.[37] The former two compounds exhibited noticeably fast Li-ionic conductivities of 2×10^{-4} S cm^{-1} at 300 K with activation energies of 0.56 and 0.26 eV, respectively.

Li-alanates, $LiAlH_4$ and Li_3AlH_6, formed by ionic bonding between Li^+ and $[AlH_4]^-$ or $[AlH_6]^{3-}$, respectively,[121–123] are also fast Li-ionic conductors.[31] The former and the latter exhibited the Li-ionic conductivities from 2×10^{-9} S cm^{-1} to 5×10^{-6} S cm^{-1} and 1×10^{-7} to 2×10^{-5} S cm^{-1}, respectively, from room temperature to 393 K.

With the complex hydrides developed to date, possible mechanisms for fast Li-ion conduction are discussed on the basis of results related to conductivity measurements at ambient[29] and ultra-high pressure,[57] NMR spectroscopic measurements[29,34,36,58], first principle molecular dynamics (FPMD) simulations[59,60] and spatially resolved Raman scattering.[61] The details are provided in a separate paper.[30]

In addition to the above report, Myrdal et al. have recently suggested that formation of the Frenkel pairs, that is, V'_{Li} and Li_i by the Kröger-Vink notation,[62] plays important role in the fast Li-ionic conduction in the pseudo-binary system, $LiBH_4$-LiI, based on the results of density functional theory (DFT) calculation coupled to quasi-elastic neutron scattering (QENS).[53] The similarity was reported in the fast Li-ionic conductor, Li_3N.[63]

Ley and co-workers recently reported the fast and a single Li-ionic conduction in $LiRE(BH_4)_3Cl$ (RE = Ce,[138] La, and Gd[139]). Despite the existences of the unreacted starting materials and the byproducts ($RECl_3$, LiCl, etc.), the materials exhibited high Li-ionic conductivities (1×10^{-4}, 2×10^{-4}, and 1×10^{-4} S cm^{-1} for RE = Ce, La, and Gd, respectively, at 293 K) with a sufficiently small contrition of electronic conductivity (less than 10^{-7} S cm^{-1}).[139] The fast Li-ionic conductions in these materials might be caused by the existence of the disordered Li-site with the occupancy of 2/3, and the continuous paths for Li-ions in their framework similar to $Li_{10}GeP_2S_{12}$[39] and $Na_2(BH_4)(NH_2)$.[32]

Yamauchi and co-workers recently examined the effect of $LiBH_4$ addition to $0.75Li_2S \cdot 0.25P_2S_5$ glass electrolytes on the Li-ionic conductivity.[64] The addition resulted in an increase in the electrical conductivity (1.6×10^{-3} S cm^{-1}) and a decrease in the activation energy (0.21 eV) than the $0.75Li_2S \cdot 0.25P_2S_5$ glass electrolyte, whose Li-ionic conductivity and activation energy are 2.7×10^{-4} S cm^{-1}and 0.26 eV, respectively. An all-solid-state TiS_2/Li cell could be stably operated for at least 5 charge–discharge cycles with a high TiS_2 utilization ratio of approximately 200 mAh g^{-1} at 298 K. The study provided a novel design principle for the development of the electrolytes for use in rechargeable batteries.

2.2. All-Solid-State Li Rechargeable Battery Assembly Using a Coated-$LiCoO_2$ Positive Electrode

Takahashi and co-workers first examined the applicability of $LiBH_4$ as a solid-state electrolyte in rechargeable Li-ion battery.[65] They used a 4 V-class $LiCoO_2$ positive electrode and Li negative electrode for the cell assembly and then the battery performance was evaluated at 393 K. At this temperature, $LiBH_4$ stays in the HT phase with a fast Li-ionic conductivity of approximately 2×10^{-3} S cm^{-1}.[29]

Although $LiBH_4$ exhibits good compatibility with Li electrodes,[30] direct contact of $LiBH_4$ with $LiCoO_2$ leads to a high interfacial resistance that exceeds 8000 Ω cm^2; this resistance has been attributed to the reaction between $LiCoO_2$ and $LiBH_4$.[65] This problem can be overcome by using a 25 nm thin-interlayer of amorphous Li_3PO_4 between $LiCoO_2$ and $LiBH_4$ (**Figure 4**). As a result, the interface resistance was reduced to approximately 16 Ω cm^2, $LiBH_4$ therefore contributed to the stable charge–discharge cycle performance.

Figure 5 shows typical charge–discharge profiles obtained at 393 K and 0.065 mA cm^{-2}. The initial discharge capacity was 89 mAh g^{-1}. Then, the 30th discharge capacity was 97% of the initial one.

This result suggests that $LiBH_4$-based complex hydride electrolytes accept the high voltage oxide-based positive electrodes by suitable surface modification, similar to sulfide-based fast Li-ionic conductors.[66–69]

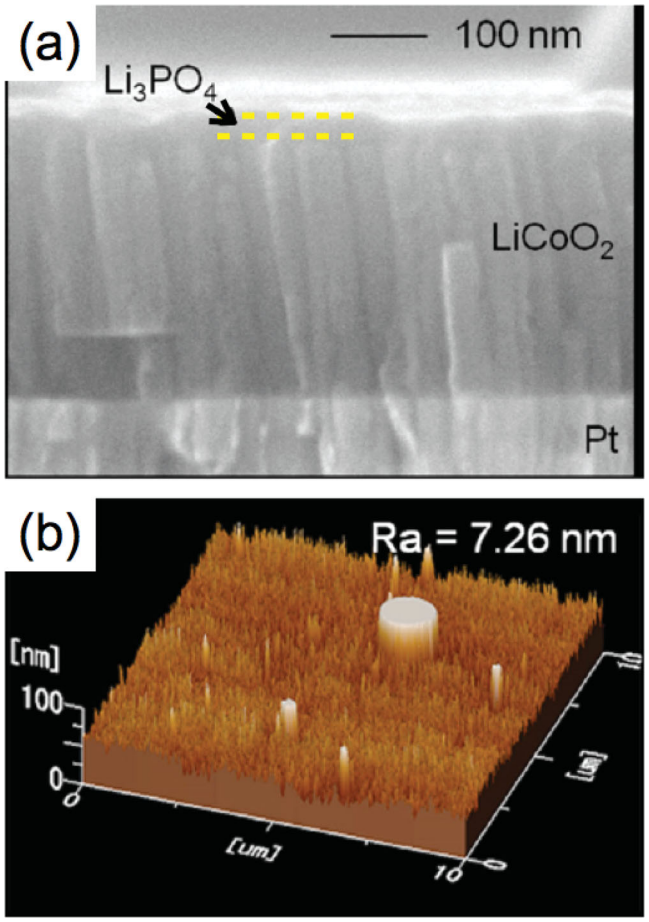

Figure 4. a) Cross-sectional scanning electron microscope (SEM) image and b) a surface scanning probe microscope image of a $LiCoO_2$ thin-film coated with an amorphous Li_3PO_4 layer. The thicknesses of the $LiCoO_2$ and Li_3PO_4 layers were 250 and 25 nm, respectively. Reproduced with permission.[65] Copyright 2013, Elsevier, Inc.

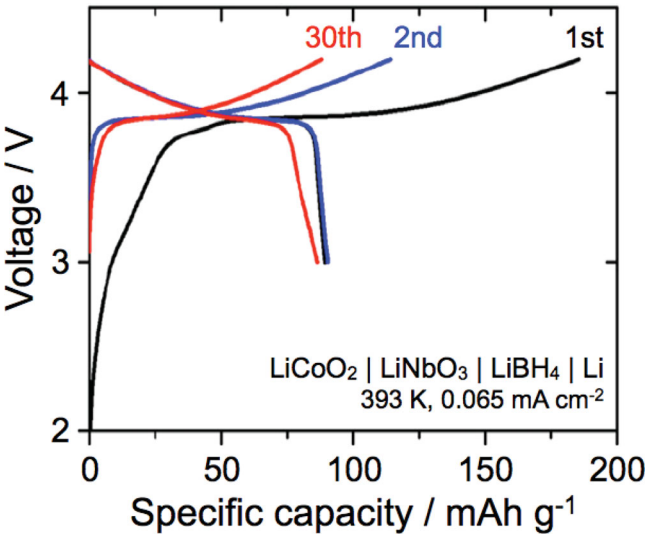

Figure 5. Charge–discharge curves of a cell with a 25 nm-thick $LiCoO_2$ thin-film. Reproduced with permission.[65] Copyright 2013, Elsevier, Inc.

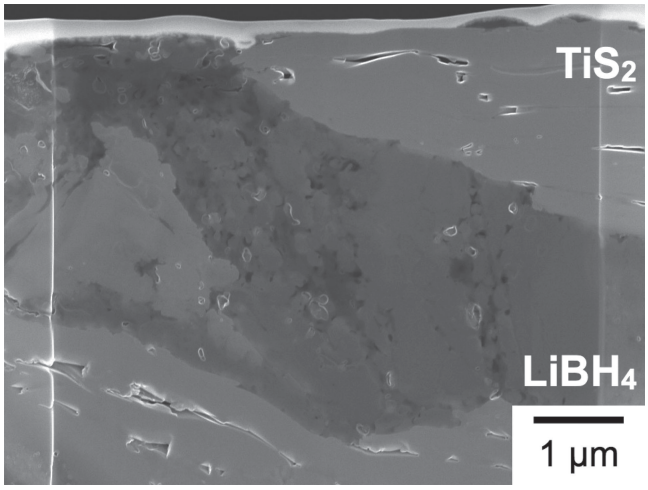

Figure 6. Cross-sectional FIB-SEM image of a TiS_2-$LiBH_4$ positive electrode.

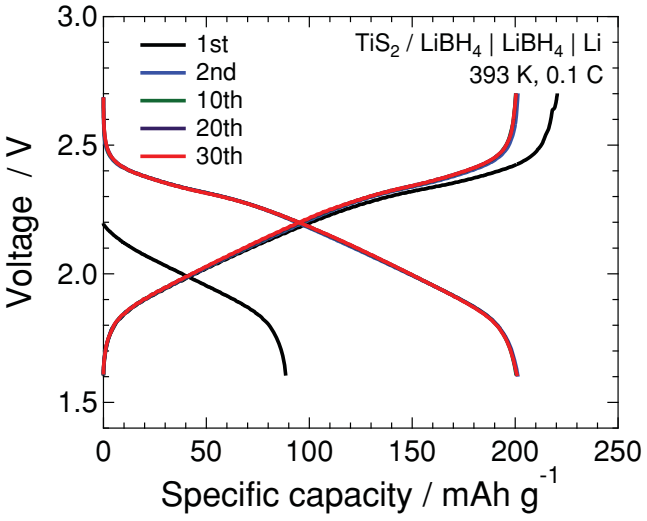

Figure 7. Typical discharge–charge profiles of a bulk-type all-solid-state Li rechargeable battery operated at 393 K and 0.1 C. TiS_2, $LiBH_4$, and Li metal were used as the positive electrode, solid-state electrolyte and negative electrode, respectively.

2.3. Bulk-type All-Solid-State Rechargeable Li Battery Assembly Using TiS_2 Positive Electrode

To further examine the validity of the use of complex hydride-based fast Li-ionic conductors as electrolytes, we assembled a bulk-type all-solid-state lithium rechargeable battery. In this study, we chose a layered dichalcogenide, TiS_2,[70–72] as the positive electrode.

Figure 6 shows a cross-sectional scanning electron microscopy equipped with focused ion-beam (FIB-SEM) image of a TiS_2–$LiBH_4$ composite positive electrode. The entire surface of TiS_2 is covered by $LiBH_4$ powders, and is thus expected to form the three-dimensional active material/electrolyte interface in the composite positive electrode. Uniaxial pressing is sufficient to form a favorable interface because of the highly deformable nature of both materials, resulting in the high TiS_2 utilization ratio during battery operation as discussed below.

The electrochemical intercalation and deintercalation of Li-ions into TiS_2 and from Li_xTiS_2, respectively, proceed as,[70,71,72]

$$TiS_2 + xLi^+ + xe^- \rightleftharpoons Li_xTiS_2 \quad (3)$$

Equation 3 predicts a theoretical capacity of 239 mAh g^{-1} when x varies from 0 to 1. **Figure 7** shows typical discharge–charge profiles of the bulk-type all-solid-state Li rechargeable battery operated at 393 K and 0.1 C (i.e., 10 h required for full-charge). During the initial discharge–charge cycle, a remarkable irreversible capacity with a low Coulombic efficiency was observed. The Coulombic efficiency then recovered to almost 100 % after the second cycle. The second discharge capacity was approximately 200 mAh g^{-1}, corresponding to the TiS_2 utilization ratio greater than 80 %. This high TiS_2-utilization ratio is achieved because of the highly deformable nature of $LiBH_4$ and TiS_2, resulting in the formation of a favorable ion transport interface between TiS_2 and $LiBH_4$ phases in the composite positive electrode.

To examine the origin of the irreversible capacity in the initial discharge–charge cycle, we performed crystal structure analysis of TiS_2, $LiBH_4$, and TiS_2–$LiBH_4$ before and after the heat treatment at 393 K for 2 h by powder XRD measurements at room temperature. Regardless of the presence or absence of $LiBH_4$, the XRD patterns of TiS_2 powders were assigned to those of the CdI_2-type structure with a space group of $P\bar{3}m1$.[73] As summarized in **Table 1**, negligible differences were observed between TiS_2 ($x = 0$ in Li_xTiS_2, open circles in **Figure 8**) and TiS_2 in the TiS_2–$LiBH_4$ mixture before heat treatment. This similarity implies that simply mixing TiS_2 and $LiBH_4$ powders with an agate mortal and an agate pestle does not affect the crystal structure of TiS_2. On the contrary, the lattice constants of TiS_2 increased by the heat treatment as shown by the open squares in Figure 8.

Dahn and Haering have systematically investigated the lattice parameters of Li_x TiS_2 as a function of x (Figure 8).[72] The lattice parameters of the TiS_2 powder agreed with previously

Table 1. Lattice constants of TiS_2 and $LiBH_4$ powders before and after the heat treatment at 393 K for 2 h.

Composition	TiS_2 (S.G.: $P\bar{3}m1$)	$LiBH_4$ (S.G.: *Pnma*)
TiS_2	$a = 0.34061(2)$	
	$c = 0.56986(7)$	
TiS_2–$LiBH_4$	$a = 0.34064(2)$	$a = 0.7174(1)$
before heat treatment	$c = 0.57004(4)$	$b = 0.44329(8)$
		$c = 0.6801(1)$
TiS_2–$LiBH_4$	$a = 0.34365(2)$	$a = 0.7171(1)$
after heat treatment	$c = 0.61901(5)$	$b = 0.44307(8)$
		$c = 0.6798(1)$
$LiBH_4$		$a = 0.71772(8)$
		$b = 0.44354(5)$
		$c = 0.68029(9)$

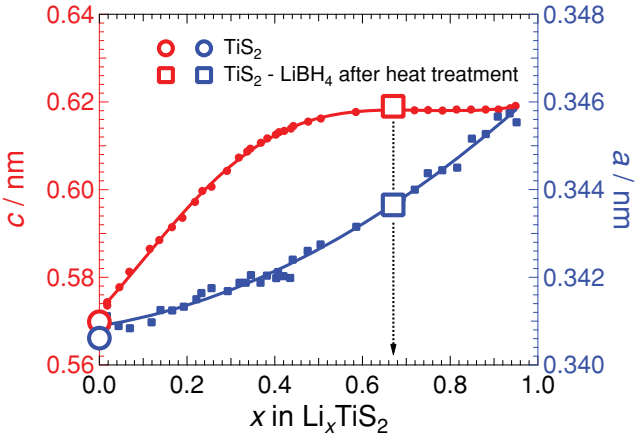

Figure 8. Lattice constants of Li_xTiS_2 as a function of *x*. Closed symbols are obtained from the literature. The open symbols are evaluated for TiS_2 and TiS_2–$LiBH_4$ composite positive electrode after the heat treatment at 393 K for 2 h. Reproduced with permission.[72] Copyright 1981, Elsevier, Ltd.

reported results. Then, the concentration of Li, that is, *x* in Li_xTiS_2, in the TiS_2-$LiBH_4$ composite powder after heat treatment was determined by the lattice parameter, *a*. The corresponding *x* was approximately 0.67, implying that the specific capacity was near 160 mAh g^{-1}.

As shown in Figure 7, the initial discharge capacity was around 90 mAh g^{-1}, which is close to the theoretical capacity (239 mAh g^{-1}) minus the estimated specific capacity due to the reaction between the TiS_2 and $LiBH_4$ powders (160 mAh g^{-1}). This result suggests that the irreversible capacity is essentially caused by the solid-state reaction of TiS_2 and $LiBH_4$ powders owing to high-temperature operation of the cells, that is, at 393 K. Gas analysis by mass spectrometry in Ar flow at elevated temperatures suggested that hydrogen started to desorb at 373 K. The molar ratio of the TiS_2–$LiBH_4$ composite was 11:89, indicating that the solid-state reaction is limited near the TiS_2 and $LiBH_4$ interfaces, and the Li species uniformly distribute in TiS_2 because of its high diffusivity.

Notably, capacity fading is quite small during battery operation. Even after 30 discharge–charge cycles, the discharge capacity remains as high as 200 mAh g^{-1}. This result suggests that the TiS_2 phase is stable despite the reducing nature of $LiBH_4$. Nearly 100 % Coulombic efficiency during battery operation suggests that the solid-state reaction and subsequent desoption of hydrogen from $LiBH_4$ hardly proceed during the long term discharge–charge cycling.

Interestingly, the bulk-type all-solid-state cell operated stably at least for 30 cycles despite the reaction between $LiBH_4$ and TiS_2 in the composite positive electrode due to high temperature operation. It is well known that the decomposition route of $LiBH_4$ is complex and it is expected that $Li_2B_{12}H_{12}$[1,74,75] and $Li_2B_{10}H_{10}$[75] are formed as the intermediate compounds during thermal decomposition. Although the decomposition route of $LiBH_4$ in the composite positive electrode was unclear in the present study, the intermediate compounds including $Li_2B_{12}H_{12}$[1,74,75] and $Li_2B_{10}H_{10}$[75] are expected to be formed at

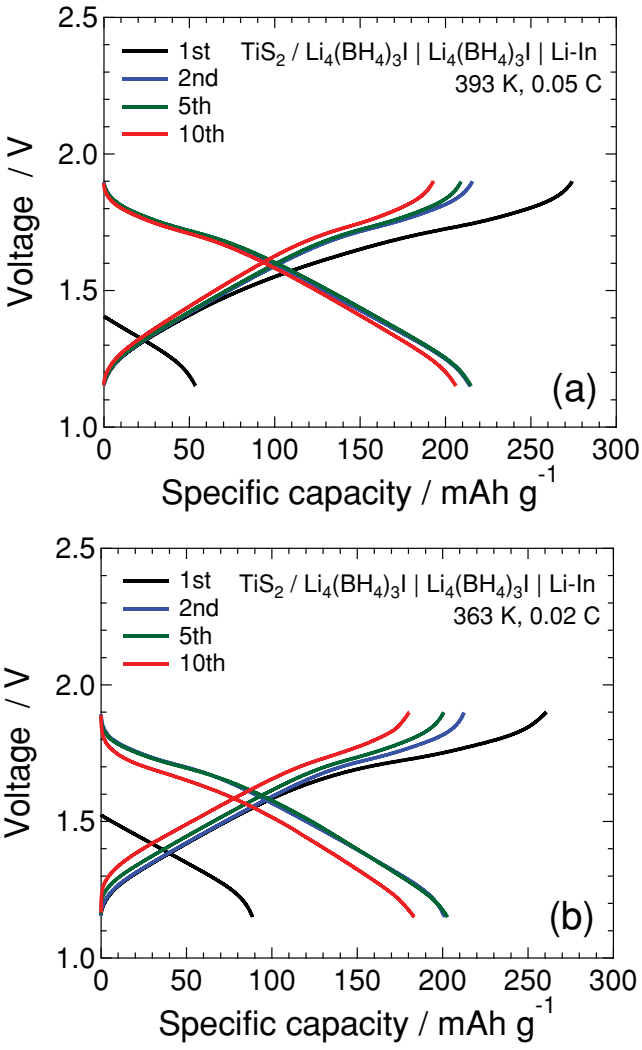

Figure 9. Typical discharge–charge profiles of bulk-type all-solid-state lithium rechargeable batteries. TiS_2, $Li_4(BH_3)I$, and Li–In alloy were used as the positive electrode, solid-state electrolyte and negative electrode, respectively. The operating temperature and C-rates are a) 393 K and 0.05 C, and b) 363 K and 0.02 C.

the TiS_2/$LiBH_4$ interface. The evaluation of the ionic conductivities in such the intermediate phases are highly required to clarify the pathways of Li-ions from $LiBH_4$ into TiS_2 as well as the interfacial reaction mechanisms during battery operation.

We extended the assembly of the bulk-type all-solid-state Li rechargeable cell using the $Li_4(BH_4)_3I$ solid-solution. Halide-doped $LiBH_4$ is also a promising candidate as the solid-state electrolyte in the lithium rechargeable batteries.[34,35] Among $LiBH_4$ doped with Li-halides,[124,125,134–136] the $Li_4(BH_4)_3I$ solid-solution exhibits fast Li-ionic conductivities of 2×10^{-3} and 6×10^{-4} S cm^{-1} at 393 and 363 K, respectively.[34]

Figure 9a,b shows typical discharge–charge profiles at 393 K and 0.05 C (i.e., 20 h required for full charge), and 363 K and 0.02 C (i.e., 50 h required for full charge), respectively, for bulk-type all-solid-state lithium rechargeable battery assembled using the $Li_4(BH_4)_3I$ electrolyte. Although irreversible capacity

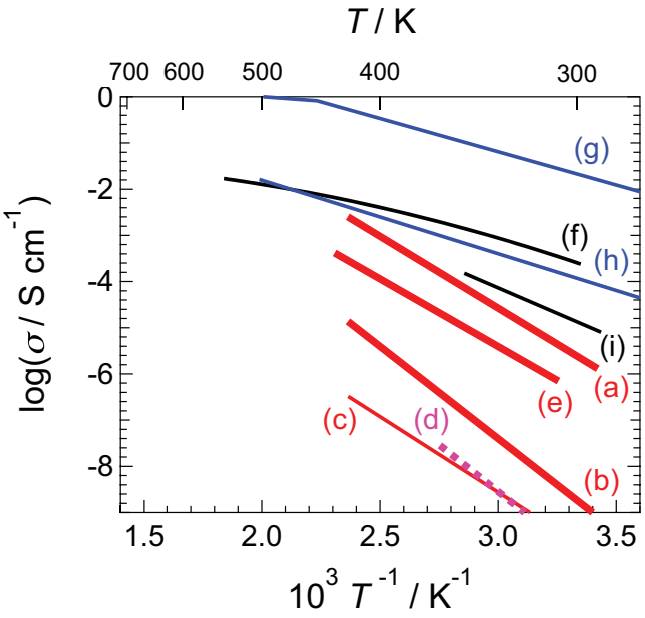

Figure 10. Electrical conductivities of various Na-ion conducting solids as functions of inverse temperature: a) $Na_2(BH_4)(NH_2)$,[32] b) $Na_2(NH_2)I$,[32] c) $Na_4(BH_4)_3I$,[32] d) $NaAlH_4$,[33] e) Na_3AlH_6,[33] f) Na_3PS_4 (glass-ceramics),[76,133] g) β''-alumina,[77] h) $Na_3Zr_2Si_2PO_{12}$ (NASICON),[78,131,132] and i) Na_2S-SiS_2 (glass).[79]

was observed during the initial discharge–charge cycles similar to the cell assembled using the $LiBH_4$ electrolyte, high TiS_2 utilization ratios were attained at both operating temperatures after the second discharge. The second discharge capacities were 215 and 200 mAh g^{-1} at 393 K and 363 K, respectively, and the tenth discharge capacities were 205 and 185 mAh g^{-1}, respectively. Contrary to the cell assembled using $LiBH_4$, a slight fading of the discharge capacities was observed at both temperatures. The long term stability as well as the origin of the discharge capacity fade need to be investigated in the future study.

The results shown in this study demonstrates the applicability of the complex hydride-based solid-state electrolytes in rechargeable batteries. Power density evaluations as well as studies on the stability of the electrolytes during the battery operation, and the compatibility between the various positive electrodes and the electrolytes are currently in progress.

3. Fast Na-Ionic Conductor Development

Despite the variety of fast Li-ionic conductors, the number of solids that exhibit fast Na-ionic conductivity is limited (**Figure 10**). From the view point of material abundance, the development of Na-ionic conductors is an emerging technological challenge. In this section, we discuss the fast Na-ionic conductivities of the complex hydrides.

3.1. Pseudo-Ternary System, $NaBH_4$-$NaNH_2$-NaI

To develop complex hydrides that exhibit fast Na-ionic conductivity, we first developed the complex hydrides on the basis of the pseudo-ternary system consisting of $NaBH_4$-$NaNH_2$-NaI[32] (see Tables S2 and S6 for the data related to the crystal structures and the conductivities, respectively).

The pseudo-binary system, $NaBH_4$ and NaI,[137] has the NaCl-type structure with a space group of $Fm\bar{3}m$. The lattice constant, a, linearly increases with increasing of the NaI concentration in $NaBH_4$, as summarized in Table S2 (Supporting Information), and the $Na(BH_4)^{1-x}I_x$ solid-solution is then formed, similar to the $LiBH_4$-LiI system,[34] as the crystal structure shown in **Figure 11**a for $x = 0.5$. The pseudo-binary system, $NaNH_2$–NaI, provides equimolar compound, $Na_2(NH_2)I$, whose crystal structure is shown in Figure 11b. It has the AgN_3-type structure with a space group of *Ibam*.

$NaBH_4$ and $NaNH_2$ also have equimolar compound, $Na_2(BH_4)(NH_2)$.[32,80,81] Somer et al. have performed detailed crystal structural analysis, which revealed that the compound experiences an order-disorder transition. The HT phase consists of the K_3SO_4F-type structure, which is an anti-perovskite-type structure with a space group of $Pm\bar{3}m$ as shown in Figure 11c. The LT phase has an ordred perovskite-type structure with a space group of *Pbcm*.[32,80] Reportedly, the transition from the LT to HT phases is very fast at 371 K, but the reverse transition is quite slow.[80] Actually, the powder XRD patterns of the synthesized $Na_2(BH_4)(NH_2)$ prepared via the mechanical ball-milling technique suggested that $Na_2(BH_4)(NH_2)$ stays as the HT phase.[32] This result also supports the observation that the phase transition from the HT to LT phase hardly occurs.[80]

Unlike $Na_2(BH_4)I$ and $Na_2(NH_2)I$ in the nominal formula, the HT $Na_2(BH_4)(NH_2)$ phase allows an occupancy of Na-sites less than unity. One-third of Na-ion sites of the $Na_2(BH_4)(NH_2)$ HT phase are disordered Na-ion vacancies.[80] Therefore, $Na_2(BH_4)(NH_2)$ exhibits fast Na-ionic conductivity based on the vacancy diffusion mechanism.[32,82] Actually, among the complex hydrides investigated in the $NaBH_4$-$NaNH_2$-NaI pseudo-ternary system, the HT phase of $Na_2(BH_4)(NH_2)$ exhibited the fastest Na-ionic conductivity from room temperature to 423 K,

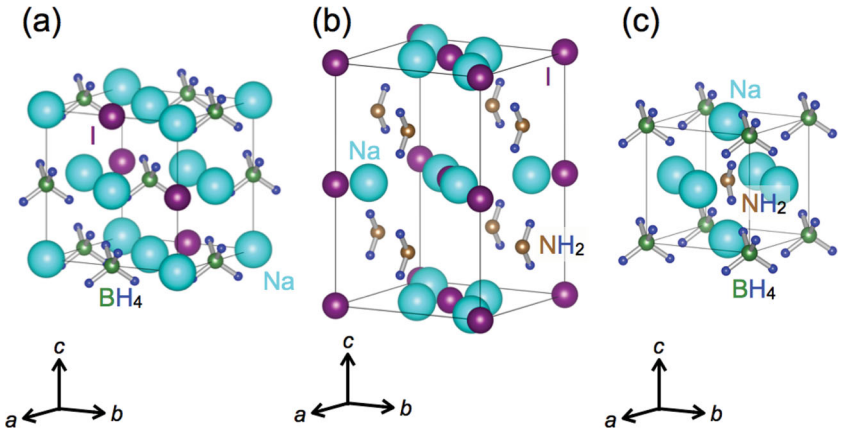

Figure 11. Crystal structures of a) $Na_2(BH_4)I$, b) $Na_2(NH_2)I$, and c) $Na_2(BH_4)(NH_2)$ (HT phase).[32] One-third of Na-ion sites in the $Na_2(BH_4)(NH_2)$ (HT phase) are disordered Na-ion vacancies.[80]

as shown in Figure 10. At 300 K, the Na-ionic conductivity of $Na_2(BH_4)(NH_2)$ is 2×10^{-6} S cm^{-1}.[32]

The dc conductivity of the Na-symmetric cell, measured by the steady-state current under a constant voltage, was 1.5×10^{-5} S cm^{-1} at 333 K. This result agrees with the bulk conductivity measured by the ac impedance measurements, implying that the $Na_2(BH_4)(NH_2)$ electrolyte and the Na electrodes form a reversible interface. On the other hand, the dc conductivity of the Mo-symmetric cell exhibited the conductivity of less than 10^{-9} S cm^{-1} because it forms a blocking interface for Na-ions. These results conclude that $Na_2(BH_4)(NH_2)$ is a single Na-ionic conductor.

Cyclic voltammograms were obtained by a two-probe technique using Na and Mo electrodes to examine the potential window of $Na_2(BH_4)(NH_2)$. The $Na_2(BH_4)(NH_2)$ electrolyte is stable even at a high voltage of 6 V *vs.* Na/Na$^+$ and shows Na dissolution and striping with high Coulombic efficiencies.[32] The latter result suggests that the $Na_2(BH_4)(NH_2)$ electrolyte is highly compatible with the Na metal electrodes.

3.2. Na-Alanates, $NaAlH_4$ and Na_3AlH_6

The complex anions, $[AlH_4]^-$ and $[AlH_6]^{3-}$, are ionically bond with Na$^+$ to form $NaAlH_4$ and Na_3AlH_6, respectively.[121,126–128,141] The crystal structures of $NaAlH_4$ and Na_3AlH_6 are shown in **Figures 12**a,b, respectively. Na-alanates exhibit noticeably fast Na-ionic conductivities,[33] as shown in Figure 10 (Tables S2 and S6 for the data related to the crystal structures and the conductivities, respectively).

Na_3AlH_6 had higher Na-ionic conductivities and smaller activation energies than $NaAlH_4$ in the investigated temperature range. The conductivity varied from 6.4×10^{-7} to 4.1×10^{-4} S cm^{-1} from room temperature to 433 K. The activation energies of Na_3AlH_6 and $NaAlH_4$ were 0.62 and 0.79 eV, respectively.[31] We noted the tendency for the absolute conductivity and the activation energy of Na_3AlH_6 to be higher and lower, respectively, than those of $NaAlH_4$, similar to Li_3AlH_6 and $LiAlH_4$, as summarized in Tables S5 and S6 (Supporting Information).

Figure 13a shows ac impedance spectra of Na- and Mo-symmetric cells obtained at 363 K. In ac impedance spectra, a semicircle appeared in a complex plane when the spectra were collected using the Na-symmetric cell. In contrast, a spike newly appeared in a lower frequency range when the symmetric cell was assembled using Mo blocking electrodes. These results imply that the semi-circle that appeared in the impedance spectra represents the electrolyte resistance. Figure 13b shows the current profile under a constant voltage. Noticeably, high steady-state currents were observed for $NaAlH_4$ and Na_3AlH_6 at 353 K when Na-electrodes were used. The dc conductivities for Na_3AlH_6 and $NaAlH_4$ were 2.3×10^{-6} and 1.4×10^{-8} S cm^{-1}, respectively, which are consistent with the bulk conductivities measured by the ac impedance measurements. The dc conductivity substantially decreased when the symmetric cells were assembled using the Mo-electrodes. They were 1.9×10^{-8} and 3.8×10^{-10} S cm^{-1} for Na_3AlH_6 and $NaAlH_4$, respectively. Van Setten et al. have performed computational calculations on the electronic structures of $NaAlH_4$ and Na_3AlH_6. They reported that the band gaps are 6.4 and 3.9 eV, respectively.[83] These results imply that both $NaAlH_4$ and Na_3AlH_6 are single Na-ionic conductors.

Efforts are devoted to investigate the defect structure and the Na-ion vacancy diffusivities in Na-alanates by the computational techniques. Contrary to $NaAlH_4$, the diffusion paths in Na_3AlH_6 are complicated. Na_3AlH_6 has eleven inequivalent jumps attributed to the two symmetry-inequivalent Na-sites, Na1 (2*b*) and Na2 (4*e*), and the different orientation of $[AlH_6]^-$ unit.[84,85] Michel and Ozolins revealed that the formation energy of the Na-vacancy, V'_{Na}, in Na1 site of Na_3AlH_6 is lower than that in $NaAlH_4$.[86] They also revealed that the Na-vacancy diffusion coefficient in Na_3AlH_6 is larger than that in $NaAlH_4$ in the temperature range from 250–400 K (The former and the latter have 1.19×10^{-12} and 4.96×10^{-11} m^2 s^{-1}, respectively, at 400 K, evaluated by the kinetic Monte Carlo simulations).[85] These might result in the higher Na-ionic conductivity in Na_3AlH_6 than in $NaAlH_4$.

Considering these results, it is expected that the complex hydrides that exhibit fast Na-ionic conductivity are also applicable in bulk-type all-solid-state rechargeable batteries similar to those exhibiting fast Li-ionic conductivity.

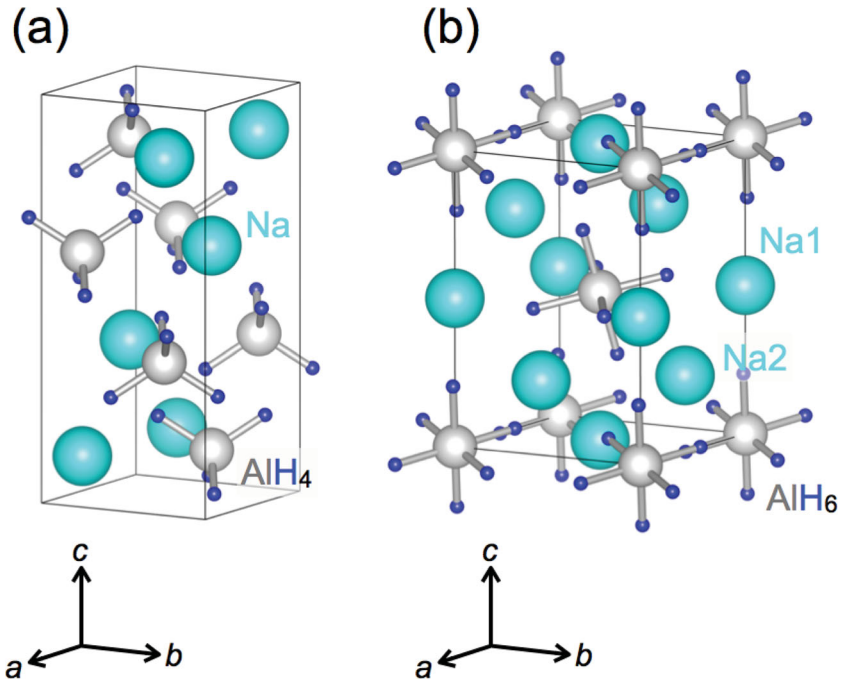

Figure 12. Crystal structures of a) $NaAlH_4$[126,141] and b) Na_3AlH_6.[128]

4. Future Prospects

In the previous section, all-solid-state Li rechargeable batteries were assembled

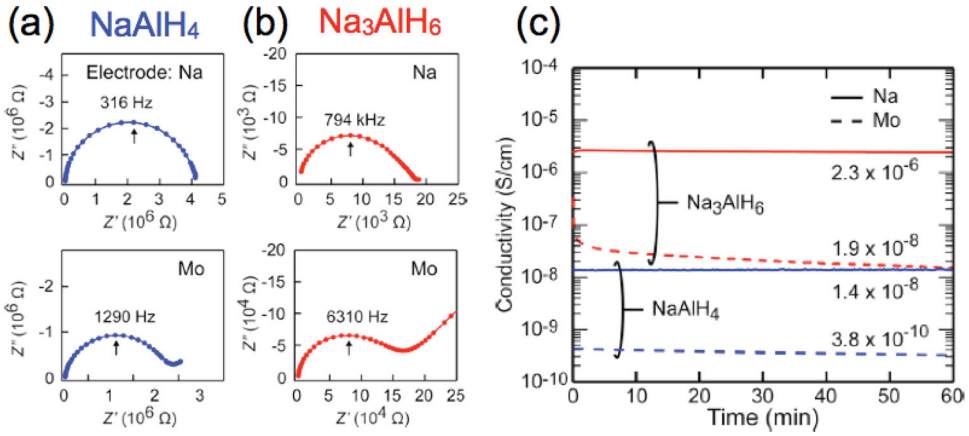

Figure 13. AC impedance spectra of the Na- and the Mo-symmetric cells assembled using a) the $NaAlH_4$ and b) the Na_3AlH_6 electrolytes at 363 K. c) The current profiles of the symmetric cells using the $NaAlH_4$ and Na_3AlH_6 electrolytes at 353 K. Reproduced with permission.[33] Copyright 2010, American Institute of Physics.

using the complex hydride-based solid-state electrolytes. Not only coated-oxides but also bare-sulfides are applicable as the positive electrode active materials. Stable charge–discharge performance validated the device concept. The fast Na-ionic conductivities in the complex hydrides suggest the possibility of an all-solid-state Na rechargeable battery. In this section, future prospects for the development of the high energy density rechargeable batteries, and the rechargeable Mg-ion batteries using the liquid and the solid-state electrolytes based on complex hydrides are briefly described.

4.1. High Energy Density Rechargeable Battery Development using Sulfur Positive Electrode

One of the important technological challenges of the all-solid-state Li rechargeable battery is the use of an elemental sulfur positive electrode. This is because a Li/S redox couple has high theoretical capacity of 1672 mAh g^{-1}, and the average discharge voltage of 2.1 V versus Li/Li^+.[87] However, this redox couple cannot be simply applied to a conventional rechargeable battery using an organic liquid electrolyte. The insulating nature of sulfur lowers the sulfur utilization ratio. In addition, the lithiated products, i.e. lithium polysulfides, are highly soluble in conventional organic liquid electrolytes, resulting in the sulfur active materials loss, and the redox shuttles.[88,89]

This issue can be addressed using a solid-state electrolyte. Nagao et al.[90] and Kobayashi et al.[91] have individually demonstrated bulk-type all-solid-state Li–S batteries. By using the sulfur-acetylene black composites and sulfide electrolytes, they achieved stable discharge–charge cycles with a high specific capacity of 900 mAh g^{-1}. Nagao et al. recently assembled a Li–S rechargeable battery using a thio-LISICON electrolyte, the composite sulfur-mesoporous carbon (CMK-3) positive electrodes, and a Li-Al negative electrode. They realized the high discharge capacity more than 1200 mAh g^{-1} after 30 charge–discharge cycles.[92,93]

Considering these results, the combinatorial use of a complex hydride-based solid-state electrolyte and a sulfur-structured carbon composites[94–102] is effective in achieving stable battery operation. In addition, the complex hydride-based solid-state electrolytes that are highly compatible with the reactive electrodes such as lithium[29,31] and sodium[32,33] are expected to enhance the energy density of the bulk-type all-solid-state Li/S[90–93] and Na/S[76,103] batteries using the positive electrodes with lower redox potentials. The techniques for the confinement of the borohydride-based hydrogen storage materials into the structured carbons[6–9] would open a route for the design of novel materials to overcome the aforementioned technological issues.

4.2. Nonaqueous and Solid-State Mg-Ionic Conductors

Mg-ions are also important ionic carriers for next generation batteries because of their high volumetric capacity of 3832 mAh cm^{-3}, their improved safety and the abundance of Mg metal. One of the challenges to realize a rechargeable Mg-ion battery is the development of suitable electrolytes.

Mohtadi et al. proposed a Mg-ion conducting nonaqueous electrolyte based on $Mg(BH_4)_2$.[104] Contrary to conventional electrolytes that contain halides,[105–107] halide-free $Mg(BH_4)_2$ enabled notable cycle performance as shown in **Figure 14**, where the Chevrel positive electrode, Mo_6S_8, and a Mg negative electrode were used for the battery assembly. Investigation of the sources of the overcharge and the capacity fading[104] as well as the overpotential would be fruitful to achieve the better battery performance. Their study provided a novel design principle for nonaqueous electrolytes for Mg-ion batteries.

With respect to developments in solid-state electrolytes with Mg-ionic conductivity, the number of reports is very limited. **Figure 15** shows Mg-ionic conductivities as functions of inverse temperature reported in previous studies. Ikeda and co-workers have reported the Mg-ionic conductivity in $MgZr_4(PO_4)_6$, which has a β-$Fe_2(SO_4)_3$ (NASICON)-type structure with monoclinic symmetry (a = 0.8895 nm, b = 0.8851 nm, c = 1.2425 nm, β = 90.60 deg., V = 0.9782 nm^3 and D = 6.51 g cm^{-3}).[108–110] The enhanced conductivity was induced by partial substitution

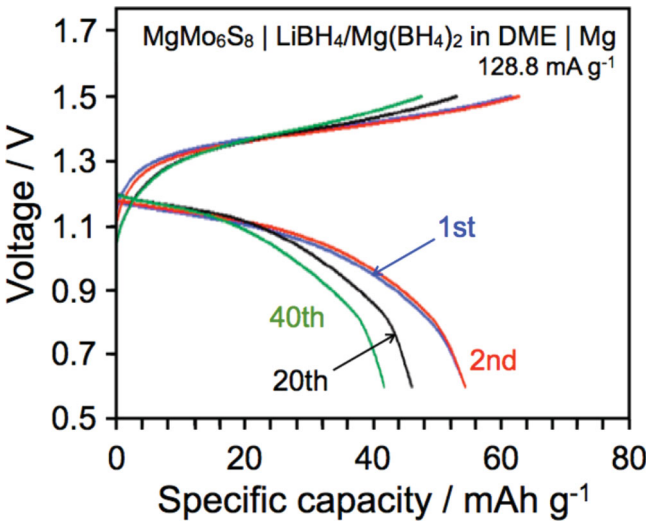

Figure 14. Charge–discharge profiles with a Mg negative electrode, a Chevrel-phase positive electrode for 3.3 molar $LiBH_4/Mg(BH_4)_2$ in DME. Reproduced with permission.[104] Copyright 2012, Wiley-VCH Verlag GmbH & Co. KGaA, Weinheim.

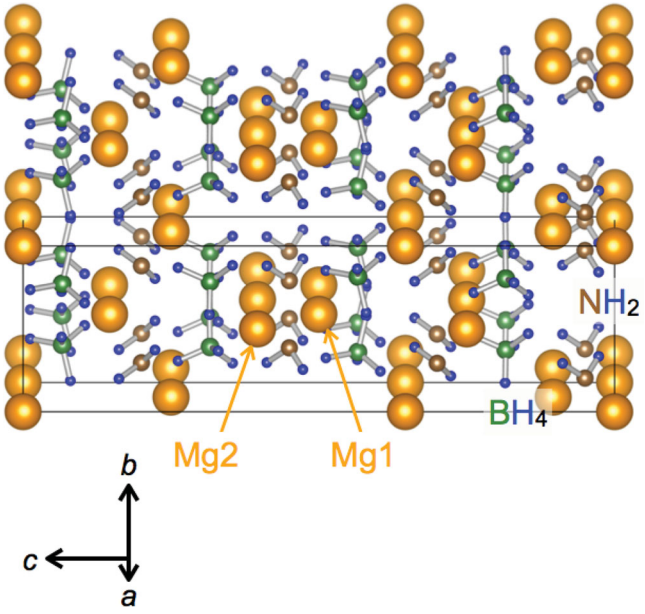

Figure 16. Crystal structure of $Mg(BH_4)(NH_2)$.[116]

of Nb into Zr-sites of $MgZr_4(PO_4)_6$.[111] Imanaka et al. have also investigated the fast Mg-ionic conductivity in composites consisting of $Mg(Zr,Nb)_4(PO_4)_6$ and $Zr_2O(PO_4)_2$.[112–114]

Recently, Higashi and co-workers have reported the fast Mg-ionic conductivity of 1.0×10^{-6} S cm^{-1} in $Mg(BH_4)(NH_2)$ at 423 K (with $\log(A_{Mg2+}/\text{S cm}^{-1}\text{ K}) = 15.8$, and $E_{a,Mg2+}/\text{eV} = 1.60$). This value is higher than $Mg(BH_4)_2$ of the order of 1×10^{-9} S cm^{-1} at that temperature (with $\log(A_{Mg2+}/\text{S cm}^{-1}\text{ K}) = 10.9$, and $E_{a,Mg2+}/\text{eV} = 14.1$).[115] Noritake et al. have determined the crystal structure of $Mg(BH_4)(NH_2)$ at 453 K as shown in **Figure 16** (i.e., a tetragonal structure with a space group of $I4_1$, $a = 0.5814(1)$ nm, $c = 2.0450(4)$ nm, $V = 0.6913(2)$ nm^3, $Z = 8$, $D = 0.9966$ g cm^{-3}).[116] The Mg-ionic conductivity of $Mg(BH_4)(NH_2)$ is higher than those reported earlier for the solid-solution[109–111] and the composites[112–114] when the conductivities are extrapolated in the lower temperature region.

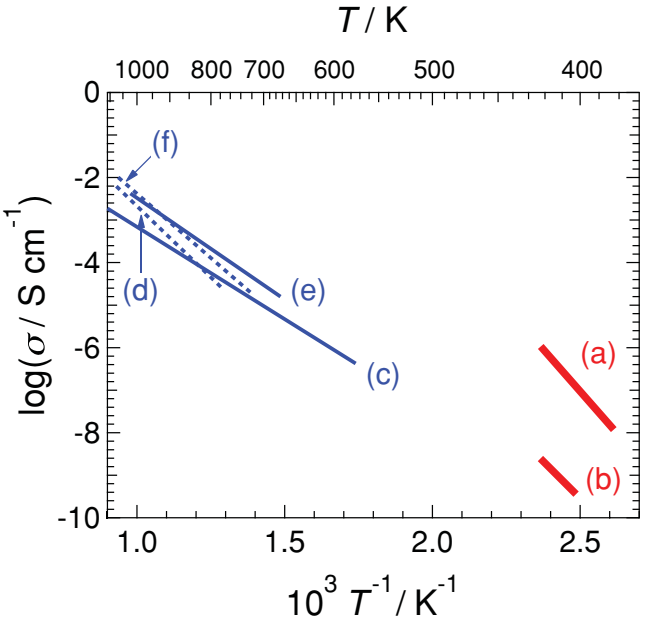

Figure 15. Electrical conductivities of various Mg-ion conducting solids as functions of inverse temperature: a) $Mg(BH_4)(NH_2)$,[115] b) $Mg(BH_4)_2$,[115] c) $MgZr_4(PO_4)_6$,[109,110] d) $Mg_{1.4}Zr_4P_6O_{24.4}$ + $0.4Zr_2O(PO_4)_2$ (composite),[112,113] e) $Mg_{0.7}(Zr_{0.85}Nb_{0.15})P_6O_{24}$,[111] and f) $Mg_{1.1}(Zr_{0.85}Nb_{0.15})_4P_6O_{24.4}$ + 0.4 $Zr_2O(PO_4)_2$ (composite).[114]

They pointed out in that $Mg(BH_4)(NH_2)$ has a Mg zigzag chain, and tunneling structure in the *a*–*b* plane. Their computational calculation results suggest that $Mg(BH_4)(NH_2)$ has two-dimensional migration paths perpendicular to the *c*-axis, and allows the formation of the Frenkel pairs that contributed to the precursor state for the Mg migration. They observed the reversible Mg deposition/striping on platinum electrodes, and the high oxidative stability at greater than 3 V vs Mg/Mg^{2+}. In addition, they observed the reasonable open circuit voltages using the Mg/S, Mg/FeS, and Mg/Ag_2S cells (1.4 V, 1.2 V, and 1.3 V, respectively, vs Mg/Mg^{2+}) compared to the results of the density functional theory (DFT) calculations.[115]

Ikeshoji and co-workers examined the effect of partial replacement of $[BH_4]^-$ by $[AlH_4]^-$ and halide-ions upon ion dynamics in $Mg(BH_4)_2$ by a FPMD simulation.[82,140] Mg-ions stay inside the tetrahedral cage consisting of four $[BH_4]^-$-units, and one $[BH_4]^-$-unit is shared by the two tetrahedral cages. This results in the coordination number of hydrogen to Mg-ion of 8.

To realize the fast Mg-ionic conduction, the displacement of Mg-ions beyond the tetrahedral cage, and the stabilization of such Mg-ions in the transition state in a space outside the tetrahedral cage are essential. This can be expected only when one of the $[BH_4]^-$ is replaced by larger $[AlH_4]^-$ that retains the numbers of hydrogen coordination to Mg-ions. The large displacement of Mg-ions cannot be expected even though $[BH_4]^-$ is replaced by the larger I^--ion. Another scenario to realize the Mg-ionic conduction is expected to be caused by the large cage

deformation. This might be resulted in the movement of Mg-ions to the center of hexahedral cage, combined by two-tetrahedral cages. When one can realize such deformations continuously, the Mg-ionic conduction may take place.[140]

The above results suggest that the preparation of the complex hydrides is a possible approach for realizing the solid-state fast Mg-ionic conductions, and thus, the all-solid-state Mg rechargeable battery developments. The use of the Mg/S redox couple as mentioned in the previous subsection is effective in enhancing the energy density of Mg rechargeable batteries.[25,117]

5. Conclusions

In this paper, we summarized the recent progress in the development of complex hydride-based fast Li- and Na-ionic conductors. The complex hydride-based fast Li-ionic conductors are applicable as bulk-type all-solid-state lithium rechargeable battery electrolytes when coated-$LiCoO_2$ and bare TiS_2 are utilized as positive electrode materials. We described the future prospects for the development of high energy density rechargeable batteries as well as Mg ion batteries in the last section of this paper. The findings related to the fast ionic conduction in the complex hydrides would open the novel design principles of the next generation batteries.

8. Experimental Section

Preparation of Electrolytes: Commercially available powders of $LiBH_4$ (>95 %, Sigma-Aldrich) and LiI (99.999 %. Sigma-Aldrich) were used as received. The $Li_4(BH_4)_3I$ solid-solution was synthesized via the mechanical ball milling technique.[34] Powdered $LiBH_4$ and LiI were weighed in a stoichiometric ratio, and then, ground using an agate mortar and an agate pestle. The mixture was transferred into a Cr-hardened steel vessel with 20 SUJ2 balls with a diameter of 7 mm. Mechanical ball milling (P-7, Fritsch) was performed for 5 h at a rotation rate of 400 rpm under an Ar atmosphere. X-ray diffraction (XRD) patterns of the powders that resulted from mechanical milling were collected using CuKα radiation at room temperature. The $Li_4(BH_4)_3I$ solid-solution was found to consist of a single phase of the HT phase of $LiBH_4$. Prior to the assembly of the all-solid-state rechargeable battery, the $LiBH_4$ and $Li_4(BH_4)_3I$ powders were ground using an agate mortar and pestle in an Ar-filled glove box.

Bulk-Type All-Solid-State Li Rechargeable Battery Assembly: TiS_2 (99.9 %, Sigma-Aldrich) was used as the positive electrode active material. Li and Li–In alloy were used as negative electrodes in the bulk-type all-solid-state rechargeable battery with $LiBH_4$ and $Li_4(BH_4)_3I$, respectively, as the electrolytes. The positive electrodes were prepared by mixing TiS_2 powders with $LiBH_4$ or $Li_4(BH_4)_3I$ using an agate mortar and pestle. The weight ratio of TiS_2:solid-state electrolyte was 2:3. The weight of the composite positive electrode was 6.0 mg. The positive electrode and 20 mg of $LiBH_4$ or 30 mg of $Li_4(BH_4)_3I$ powders were placed together into an 8-mm-diameter die, and then uniaxially pressed at 240 MPa. The resultant compact was placed into a stainless steel vessel, and then, a Li film or a Li-In bi-layer film was placed opposite the positive electrode. For cells using Li–In negative electrodes, the cell was heated at 393 K for a few hours to proceed the formation of a Li–In alloy. Discharge–charge characteristics were evaluated by applying a constant current mode. The evaluation of the all-solid-state battery assembled using $LiBH_4$ was conducted at 393 K and 0.1 C in the voltage range of 1.6–2.7 V at 0.1 C. The evaluation of the battery with the $Li_4(BH_4)_3I$ electrolyte was conducted at 0.05 and 0.02 C at 393 and 363 K, respectively, in the voltage range of 1.15–1.9 V. A cross-sectional view of the positive electrode, TiS_2–$LiBH_4$, was observed by field-emission scanning electron microscopy (SU9000, Hitachi High-Technologies Corporation) equipped with a focused ion beam (FB2200, Hitachi High-Technologies Corporation). To examine the reactivity between $LiBH_4$ and TiS_2, powder XRD measurements were conducted for TiS_2, $LiBH_4$, and TiS_2–$LiBH_4$ composites before and after heat treatment at 393 K for 2 h in an Ar-filled environment at room temperature. The lattice constants were determined by using the TREOR program.[119]

Supporting Information

Supporting Information is available from the Wiley Online Library or from the author.

Acknowledgements

Figures 1,11,12,15 and 16 were drawn using the VESTA program.[118] The authors thank G. Nogami, M. Tazawa, and Dr. M. Taniguchi at Mitsubishi Gas Chemicals Co Ltd. for the FIB-SEM analysis. Fruitful discussion with Dr. S. Higashi, Dr. K. Takechi, and Dr. K. Miwa of Toyota Central R&D Labs, Inc., and valuable collaboration and communication with Late Prof. H. Maekawa, Prof. H. Takamura, Dr. H. Oguchi, Dr. T. Sato, Dr. S. Takagi, Dr. T. Ikeshoji, Dr. K. Aoki, H. Ohmiya, and N. Warifune of Tohoku University are highly appreciated. The authors gratefully acknowledge financial support from the Target Project of Advanced Institute for Materials Research (WPI-AIMR) and the Integrated Materials Research Center for a Low-Carbon Society (LC-IMR), Tohoku University, JSPS KAKENHI Grant Number 25220911, and Advanced Low Carbon Technology Research and Development Program (ALCA) from Japan Science and Technology Agency (JST).

Received: September 10, 2013
Revised: October 31, 2013
Published online: January 9, 2014

[1] S. Orimo, Y. Nakamori, J. R. Eliseo, A. Züttel, C. M. Jensen, *Chem. Rev.* **2007**, *107*, 4111–4132.
[2] A. Züttel, P. Wenger, S. Rentsch, P. Sudan, P. Mauron, C. Emmenegger, *J. Power Sources* **2003**, *118*, 1–7.
[3] S. Orimo, Y. Nakamori, G. Kitahara, K. Miwa, N. Ohba, S. Towata, A. Züttel, *J. Alloy Compd.* **2005**, *404-406*, 427–430.
[4] Y. Nakamori, K. Miwa, A. Ninomiya, H. Li, N. Ohba, S. Towata, A. Züttel, S. Orimo, *Phys. Rev. B* **2006**, *74*, 045126.
[5] M. Au, A. Jurgensen, K. Zeigler, *J. Phys. Chem. B* **2006**, *110*, 26482–26487.
[6] A. F. Gross, J. J. Vajo, S. L. Van Atta, G. L. Olson, *J. Phys. Chem. C* **2008**, *112*, 5651–5657.
[7] T. K. Nielsen, U. Bosenberg, R. Gosalawit, M. Dornheim, Y. Cerenius, F. Besenbacher, T. R. Jensen, *ACS Nano* **2010**, *4*, 3903–3908.
[8] X. Liu, D. Peaslee, C. Z. Jost, E. H. Majzoub, *J. Phys. Chem. C* **2010**, *114*, 14036–14041.
[9] P. Ngene, P. Adelhelm, A. M. Beale, K. P. de Jong, P. E. de Jongh, *J. Phys. Chem. C* **2010**, *114*, 6163–6168.
[10] J. J. Vajo, S. L. Skeith, F. Mertens, *J. Phys. Chem. B* **2005**, *109*, 3719–3722.
[11] G. Barkhordarian, T. Klassen, M. Dornheim, R. Bormann, *J. Alloy Compd.* **2007**, *440*, L18–L21.
[12] F. E. Pinkerton, M. S. Meyer, G. P. Meisner, M. P. Balogh, J. J. Vajo, *J. Phys. Chem. C* **2007**, *111*, 12881–12885.
[13] T. Nakagawa, T. Ichikawa, N. Hanada, Y. Kojima, H. Fujii, *J. Alloy Compd.* **2007**, *446-447*, 306–309.

[14] S.-A. Jin, Y.-S. Lee, J.-H. Shim, Y. W. Cho, *J. Phys. Chem. C* **2008**, *112*, 9520–9524.
[15] O. Friedrichs, J. W. Kim, A. Remhof, F. Buchter, A. Borgschulte, D. Wallacher, Y. W. Cho, M. Fichtner, K. H. Oh, A. Züttel, *Phys. Chem. Chem. Phys.* **2009**, *11*, 1515–1520.
[16] J.-P. Soulie, G. Genaudin, R. Cerny, K. Yvon, *J. Alloy Compd.* **2002**, *346*, 200–205.
[17] Y. Oumellal, A. Rougier, G. A. Nazri, J.-M. Tarascon, L. Aymard, *Nat. Mater.* **2008**, *7*, 916–921.
[18] W. Zaidi, Y. Oumellal, J.-P. Bonnet, J. Zhang, F. Cuevas, M. Latroche, J.-L. Bobet, L. Amard, *J. Power Sources* **2011**, *196*, 2854–2857.
[19] Y. Oumellal, A. Rougier, J.-M. Tarascon, L. Aymard, *J. Power Sources* **2009**, *192*, 698–702.
[20] N. Hanada, A. Kamura, H. Suzuki, K. Takai, T. Ichikawa, Y. Kojima, *J. Alloy Compd.* **2011**, *509S*, S584–S587.
[21] Y. Oumellal, W. Zaidi, J.-P. Bonnet, F. Cuevas, M. Latroche, J. Zhang, J.-L. Bobet, A. Rougier, L. Aymard, *Int. J. Hydrogen Energy* **2012**, *37*, 7831–7835.
[22] W. Zaidi, J.-P. Bonnet, J. Zhang, F. Cuevas, M. Latroche, S. Couillaud, J.-L. Bobet, M. T. Sougrati, J. C. Jumas, L. Aymard, *Int. J. Hydrogen Energy* **2013**, *38*, 4798–4808.
[23] J. Zhang, W. Zaidi, V. Paul-Boncour, K. Provost, A. Michalowicz, F. Cuevavs, M. Latroche, S. Belin, J.-P. Bonnet, L. Aymard, *J. Mater. Chem. A* **2013**, *1*, 4706–4717.
[24] J. F. M. Oudenhoven, L. Baggetto, P. H. L. Notten, *Adv. Energy Mater.* **2011**, *1*, 10–33.
[25] M. Armand, J.-M. Tarascon, *Nature* **2008**, *451*, 652–657.
[26] K. Takada, *Acta Mater.* **2013**, *61*, 759–770.
[27] Y. Kato, K. Kawamoto, R. Kanno, M. Hirayama, *Electrochemistry* **2012**, *80*, 749–751.
[28] J. W. Fergus, *J. Power Sources* **2010**, *195*, 4554–4569.
[29] M. Matsuo, Y. Nakamori, S. Orimo, H. Maekawa, H. Takamura, *Appl. Phys. Lett.* **2007**, *91*, 224103.
[30] M. Matsuo, S. Orimo, *Adv. Energy Mater.* **2011**, *1*, 161–172.
[31] H. Oguchi, M. Matsuo, T. Sato, H. Takamura, H. Maekawa, H. Kuwano, S. Orimo, *J. Appl. Phys.* **2010**, *107*, 096104.
[32] M. Matsuo, S. Kuromoto, T. Sato, H. Oguchi, H. Takamura, S. Orimo, *Appl. Phys. Lett.* **2012**, *100*, 203904.
[33] H. Oguchi, M. Matsuo, S. Kuromoto, H. Kuwano, S. Orimo, *J. Appl. Phys.* **2012**, *111*, 036102.
[34] H. Maekawa, M. Matsuo, H. Takamura, M. Ando, Y. Noda, T. Karahashi, S. Orimo, *J. Am. Chem. Soc.* **2009**, *131*, 894–895.
[35] M. Matsuo, H. Takamura, H. Maekawa, H.-W. Li, S.-i. Orimo, *Appl. Phys. Lett.* **2009**, *94*, 084103.
[36] M. Matsuo, A. Remhof, P. Martelli, R. Caputo, M. Ernst, Y. Miura, T. Sato, H. Oguchi, H. Maekawa, H. Takamura, A. Borgschulte, A. Züttel, S. Orimo, *J. Am. Chem. Soc.* **2009**, *131*, 16389–16391.
[37] M. Matsuo, T. Sato, Y. Miura, H. Oguchi, Y. Zhou, H. Maekawa, H. Takamura, S. Orimo, *Chem. Mater.* **2010**, *22*, 2702–2704.
[38] W. Li, G. Wu, Z. Xiong, Y. P. Feng, P. Chen, *Phys. Chem. Chem. Phys.* **2012**, *14*, 1596-1606.
[39] N. Kamaya, K. Homma, Y. Yamakawa, M. Hirayama, R. Kanno, M. Yonemura, T. Kamiyama, Y. Kato, S. Hama, K. Kawamoto, A. Mitsui, *Nat. Mater.* **2011**, *10*, 682–686.
[40] F. Mizuno, A. Hayashi, K. Tadanaga, M. Tatsumisago, *Adv. Mater.* **2005**, *17*, 918–921.
[41] S. Kondo, K. Takada, Y. Yamamura, *Solid State Ionics* **1992**, *53-56*, 1183–1186.
[42] M. Tatsumisago, K. Hirai, T. Minami, K. Takada, S. Kondo, *J. Ceram. Soc. Jpn.* **1993**, *101*, 1315–1317.
[43] R. Kanno, M. Murayama, *J. Electrochem. Soc.* **2001**, *148*, A742–A746.
[44] H. Y.-P. Hong, *Mater. Res. Bull.* **1978**, *13*, 117–124.
[45] U. V. Alphen, M. F. Bell, W. Wichelhaus, *Electrochim. Acta* **1978**, *23*, 1395–1397.
[46] Y. Inaguma, C. Liquan, M. Itoh, T. Nakamura, T. Uchida, H. Ikuta, M. Wakihara, *Solid State Commun.* **1993**, *86*, 689–693.
[47] R. Murugan, V. Thangadurai, W. Weppner, *Angew. Chem. Int. Ed.* **2007**, *46*, 7778–7781.
[48] H. Aono, E. Sugimoto, Y. Sadaoka, N. Imanaka, G. Adachi, *J. Electrochem. Soc.* **1989**, *136*, 590–591.
[49] K. Miwa, N. Ohba, S. Towata, *Phys. Rev. B* **2004**, *69*, 245120.
[50] E. Orgaz, A. Membrillo, R. Castaneda, A. Aburto, *J. Alloy Compd.* **2005**, *404-406*, 176–180.
[51] H. Oguchi, M. Matsuo, J. S. Hummelshoj, T. Vegge, J. K. Norskov, T. Sato, Y. Miura, H. Takamura, H. Maekawa, S. Orimo, *Appl. Phys. Lett.* **2009**, *94*, 141912.
[52] D. Sveinbjornsson, J. S. G. Myrdal, D. Blanchard, J. J. Bentzen, T. Hirata, M. B. Mogensen, P. Norby, S. Orimo, T. Vegge, *J. Phys. Chem. C* **2013**, *117*, 3249–3257.
[53] J. S. G. Myrdal, D. Blanchard, D. Sveinbjornsson, T. Vegge, *J. Phys. Chem. C* **2013**, *117*, 9084–9091.
[54] C. C. Stephenson, D. W. Rice, W. H. Stockmayer, *J. Chem. Phys.* **1955**, *23*, 1960.
[55] Y. Filinchuk, D. Chernyshov, R. Cerny, *J. Phys. Chem. C* **2008**, *112*, 10579–10584.
[56] F. Buchter, Z. Lodziana, P. Mauron, A. Remhof, O. Friedrichs, A. Borgshulte, A. Züttel, D. Sheptyakov, T. Strassel, A. J. Ramirez-Cuesta, *Phys. Rev. B* **2008**, *78*, 094302.
[57] H. Takamura, Y. Kuronuma, H. Maekawa, M. Matsuo, S. Orimo, *Solid State Ionics* **2011**, *192*, 118–121.
[58] V. Epp, M. Wilkening, *Phys. Rev. B* **2010**, *82*, 020301.
[59] T. Ikeshoji, E. Tsuchida, K. Ikeda, M. Matsuo, H.-W. Li, Y. Kawazoe, S. Orimo, *Appl. Phys. Lett.* **2009**, *95*, 221901.
[60] T. Ikeshoji, E. Tsuchida, T. Morishita, K. Ikeda, M. Matsuo, Y. Kawazoe, S. Orimo, *Phys. Rev. B* **2011**, *83*, 144301.
[61] A. Borgschulte, R. Gremaud, S. Kato, N. P. Stadie, A. Remhof, A. Züttel, M. Matsuo, S. Orimo, *Appl. Phys. Lett.* **2010**, *97*, 031916.
[62] F. A. Kröger, H. J. Vink, In *Crystalline Solids, Solid State Physics*, Vol. *3*, (Eds: F. Seitz, D. Turnbull) Academic Press Inc, New York, **1956.**
[63] H. Shulz, K. H. Thiemann, *Acta Crystallogr. A* **1979**, *35*, 309–314.
[64] A. Yamauchi, A. Sakuda, A. Hayashi, M. Tatsumisago, *J. Power Sources* **2013**, *244*, 707–710.
[65] K. Takahashi, K. Hattori, T. Yamazaki, K. Takada, M. Matsuo, S. Orimo, H. Maekawa, H. Takamura, *J. Power Sources* **2013**, *226*, 61–64.
[66] N. Ohta, K. Takada, I. Sakaguchi, L. Zhang, R. Ma, K. Fukuda, M. Osada, T. Sasaki, *Electrochem. Commun.* **2007**, *9*, 1486–1490.
[67] A. Sakuda, A. Hayashi, M. Tatsumisago, *Chem. Mater.* **2010**, *22*, 949–956.
[68] K. Takada, N. Ohta, L. Zhang, X. Xu, H. T. Hang, T. Ohnishi, M. Osada, T. Sasaki, *Solid State Ionics* **2012**, *225*, 594–597.
[69] K. Takada, N. Ohta, L. Zhang, K. Fukuda, I. Sakaguchi, R. Ma, M. Osada, S. Takayoshi, *Solid State Ionics* **2008**, *179*, 1333–1337.
[70] M. S. Whittingham, *Science* **1976**, *192*, 1126–1127.
[71] M. S. Whittingham, *Prog. Solid State Chem.* **1978**, *12*, 41–99.
[72] J. R. Dahn, R. R. Haering, *Solid State Commun.* **1981**, *40*, 245–248.
[73] R. R. Chianelli, J. C. Scanlon, A. H. Thompson, *Mater. Res. Bull.* **1975**, *10*, 1379–1382.
[74] S. Orimo, Y. Nakamori, N. Ohba, K. Miwa, M. Aoki, S. Towata, A. Züttel, *Appl. Phys. Lett.* **2006**, *89*, 021920.
[75] O. Friedrichs, A. Remhof, S.-J. Hwang, A. Züttel, *Chem. Mater.* **2010**, *22*, 3265–3268.
[76] A. Hayashi, K. Noi, A. Sakuda, M. Tatsumisago, *Nat. Commun.* **2012**, *3*, 856.
[77] J. P. Boilot, G. Collin, P. Colomban, R. Comes, *Phys. Rev. B* **1980**, *22*, 5912–5923.

[78] J. B. Goodenough, H. Y.-P. Hong, J. A. Kafalas, *Mater. Res. Bull.* **1976**, *11*, 203–220.
[79] M. Ribes, B. Barrau, J. L. Souquet, *J. Non-Cryst. Solids* **1980**, *38/39*, 271–276.
[80] M. Somer, S. Acar, C. Koz, I. Kokal, P. Hohn, R. Gardoso-Gil, U. Aydemir, L. Akselrud, *J. Alloy Compd.* **2010**, *491*, 98–105.
[81] P. A. Chater, P. A. Anderson, J. W. Prendergast, A. Walton, V. S. J. Mann, D. Book, W. I. F. David, S. R. Johnson, P. P. Edwards, *J. Alloy Compd.* **2007**, *446-447*, 350–354.
[82] M. Matsuo, H. Oguchi, T. Sato, H. Takamura, E. Tsuchida, T. Ikeshoji, S. Orimo, *J. Alloy Compd.* **2013**, *580*, S98–S101.
[83] M. J. van Setten, V. A. Popa, G. A. de Wijs, G. Brocks, *Phys. Rev. B* **2007**, *75*, 035204.
[84] J. Voss, Q. Shi, H. S. Jacobsen, M. Zamponi, K. Lefmann, T. Vegge, *J. Phys. Chem. B* **2007**, *111*, 3886–3892.
[85] K. J. Michel, V. Ozolins, *J. Phys. Chem C* **2011**, *115*, 21465–21472.
[86] K. J. Michel, V. Ozolins, *J. Phys. Chem. C* **2011**, *115*, 21443–21453.
[87] J. Wnag, J. Yang, C. Wang, K. Du, J. Xie, N. Xu, *Adv. Funct. Mater.* **2003**, *13*, 487–492.
[88] R. D. Rauh, F. S. Shuker, J. M. Marston, S. B. Brummer, *J. Inorg. Nucl. Chem.* **1977**, *39*, 1761–1766.
[89] S. S. Zhang, *J. Power Sources* **2013**, *231*, 153–162.
[90] M. Nagao, A. Hayashi, M. Tatsumisago, *Electrochem. Commun.* **2012**, *22*, 177–180.
[91] T. Kobayashi, Y. Imade, D. Shishihara, K. Homma, M. Nagao, R. Watanabe, T. Yokoi, A. Yamada, R. Kanno, T. Tatsumi, *J. Power Sources* **2008**, *182*, 621–625.
[92] M. Nagao, Y. Imade, H. Narisawa, T. Kobayashi, R. Watanabe, T. Yokoi, T. Tatsumi, R. Kanno, *J. Power Sources* **2013**, *222*, 237–242.
[93] M. Nagao, Y. Imade, H. Narisawa, R. Watanabe, T. Yokoi, T. Tatsumi, R. Kanno, *J. Power Sources* **2013**, *243*, 60–64.
[94] X. Ji, K. T. Lee, L. F. Nazar, *Nat. Mater.* **2009**, *8*, 500–506.
[95] J. Wang, S. Y. Chew, Z. W. Zhao, S. A. Ashraf, D. Wexler, J. Chen, S. H. Ng, S. L. Chou, H. K. Liu, *Carbon* **2008**, *46*, 229–235.
[96] M. Rao, W. Li, E. J. Cairns, *Electrochem. Commun.* **2012**, *17*, 1–5.
[97] N. Tachikawa, K. Yamauchi, E. Takashima, J.-W. Park, K. Dokko, M. Watanabe, *Chem. Commun.* **2011**, *47*, 8157–8159.
[98] M. Rao, X. Geng, X. Li, S. Hu, W. Lu, *J. Power Sources* **2012**, *212*, 179–185.
[99] H. Ogawa, A. Unemoto, I. Honma, *Electrochemistry* **2012**, *80*, 765–767.
[100] A. Unemoto, H. Ogawa, Y. Gambe, I. Honma, *Electrochim. Acta*, unpublished.
[101] H. Wang, Y. Yang, Y. Liang, J. T. Robinson, Y. Li, A. Jackson, Y. Cui, H. Dai, *Nano Lett.* **2011**, *11*, 2644–2647.
[102] L. Ji, M. Rao, H. Zheng, L. Zhang, Y. Li, W. Duan, J. Guo, E. J. Cairns, Y. Zhang, *J. Am. Chem. Soc.* **2011**, *133*, 18522–18525.
[103] K. B. Hueso, M. Armand, T. Rojo, *Energy Environ. Sci.* **2013**, *6*, 734–749.
[104] R. Mohtadi, M. Matsui, T. S. Arthur, S.-J. Hwang, *Angew. Chem. Int. Ed.* **2012**, *51*, 9780–9783.
[105] D. Aurbach, Z. Lu, A. Schechter, Y. Gofer, H. Gizbar, R. Turgeman, Y. Cohen, M. Moshkovich, E. Levi, *Nature* **2000**, *407*, 724–727.
[106] N. Amir, Y. Vestfrid, O. Chusid, Y. Gofer, D. Aurbach, *J. Power Sources* **2007**, *174*, 1234–1240.
[107] J. Muldoon, C. B. Bucur, A. G. Oliver, T. Sugimoto, M. Matsui, H. S. Kim, G. D. Allred, J. Zajicek, Y. Kotani, *Energy Environ. Sci.* **2012**, *5*, 5941–5950.
[108] K. Nomura, S. Ikeda, K. Ito, H. Einaga, *J. Electroanal. Chem.* **1992**, *326*, 351–356.
[109] S. Ikeda, M. Takahashi, J. Ishikawa, K. Ito, *Solid State Ionics* **1987**, *23*, 125–129.
[110] K. Nomura, S. Ikeda, K. Ito, H. Einaga, *Bull. Chem. Soc. Jpn.* **1992**, *65*, 3221–3227.
[111] N. Imanaka, Y. Okazaki, G. Adachi, *Electrochem. Solid-State* **2000**, *3*, 327–329.
[112] N. Imanaka, Y. Okazaki, G. Adachi, *Chem. Lett.* **1999**, 939–940.
[113] N. Imanaka, Y. Okazaki, G. Adachi, *J. Mater. Chem.* **2000**, *10*, 1431–1435.
[114] N. Imanaka, Y. Okazaki, G. Adachi, *Ionics* **2001**, *7*, 440–446.
[115] S. Higashi, K. Miwa, M. Aoki, K. Takechi, unpublished.
[116] T. Noritake, K. Miwa, M. Aoki, M. Matsumoto, S. Towata, H.-W. Li, S. Orimo, *Int. J. Hydrogen Energ.* **2013**, *38*, 6730–6735.
[117] H. S. Kim, T. S. Arthur, G. D. Allred, J. Zajicek, J. G. Newman, A. E. Rodnyansky, A. G. Oliver, W. C. Boggess, J. Muldoon, *Nat. Commun.* **2011**, *2*, 427.
[118] K. Momma, F. Izumi, *Commission on Crystallogr. Comput., IUCr Newslett., No. 7* **2006**, 106–119.
[119] L. Eriksson, M. Westdahl, *J. Appl. Cryst.* **1985**, *18*, 367–370.
[120] J. B. Yang, X. D. Zhou, Q. Cai, W. J. James, W. B. Yelon, *Appl. Phys. Lett.* **2006**, *88*, 041914.
[121] T. Sato, K. Ikeda, H.-W. Li, H. Yukawa, M. Morinaga, S. Orimo, *Mater. Trans.* **2009**, *50*, 182–186.
[122] B. C. Hauback, H. W. Brinks, H. Fjellvag, *J. Alloy Compd.* **2002**, *346*, 184–189.
[123] H. W. Brinks, B. C. Hauback, *J. Alloy Compd.* **2003**, *354*, 143–147.
[124] H. Ott, *Phys. Zeitschrift* **1923**, *24*, 209–213.
[125] D. Fischer, A. Mueller, M. Jansen, *Z. Anorg. Allg. Chem.* **2004**, *630*, 2697–2700.
[126] B. C. Hauback, H. W. Brinks, C. M. Jensen, K. Murphy, A. J. Maeland, *J. Alloy Compd.* **2003**, *358*, 142–145.
[127] V. Ozolins, E. H. Majzoub, T. J. Udovic, *J. Alloy Compd.* **2004**, *375*, 1–10.
[128] E. Ronnebro, D. Noreus, K. Kadir, A. Reiser, B. Bogdanovic, *J. Alloy Compd.* **2000**, *299*, 101–106.
[129] C. A. Geiger, E. Alekseev, B. Lazic, M. Fisch, T. Armbruster, R. Langner, M. Fechtelkord, N. Kim, T. Pettke, W. Weppner, *Inorg. Chem.* **2011**, *50*, 1089–1097.
[130] J. Ibarra, A. Varez, C. Leon, J. Santamaria, L. M. Torres-Martinez, J. Sanz, *Solid State Ionics* **2000**, *134*, 219–228.
[131] W. H. Baur, J. R. Dygas, D. H. Whitmore, J. Faber, *Solid State Ionics* **1986**, *18/19*, 935–943.
[132] J.-J. Didisheim, E. Prince, B. J. Wuensch, *Solid State Ionics* **1986**, *18/19*, 944–958.
[133] M. Jansen, U. Henseler, *J. Solid State Chem.* **1992**, *99*, 110–119.
[134] R. Court-Castagnet, C. Kaps, C. Cros, P. Hagenmuller, *Solid State Ionics* **1993**, *61*, 327–334.
[135] P. Manoravi, K. Shahi, *Solid State Ionics* **1992**, *58*, 243–248.
[136] C. C. Liang, *J. Electrochem. Soc.* **1973**, *120*, 1289–1292.
[137] P. Manoravi, K. Shahi, *J. Phys. Chem. Solids* **1991**, *52*, 527–535.
[138] M. B. Ley, D. B. Ravnsbak, Y. Filinchuk, Y.-S. Lee, R. Janot, Y. W. Cho, J. Skibsted, T. R. Jensen, *Chem. Mater.* **2012**, *24*, 1654–1663.
[139] M. B. Key, S. Boulineau, R. Janot, Y. Filinchuk, T. R. Jensen, *J. Phys. Chem. C* **2012**, *116*, 21267–21276.
[140] T. Ikeshoji, E. Tsuchida, S. Takagi, M. Matsuo, S. Orimo, *RSC Adv.* **2014**, *4*, 1366–1370.
[141] B. C. Hauback, *Z. Kristallogr.* **2008**, *223*, 636–648.